Applied Chemistry Today **19(73)** (2024) 73-90

Semnan University

Applied Chemistry Today

Journal homepage: https://chemistry.semnan.ac.ir/

ISSN: 2981-2437

Research Article

Synthesis of Zinc Oxide-based nanocomposites for photocatalytic removal of contaminant

Maryam Tondkar Mobaraki[a], Hassan Zavvar Mousavi[a], Hadi Fallah Moafi[a,*], Mohammad Moghadam[b]

[a]Department of Inorganic Chemistry, Faculty of Chemistry, University of Guilan, Rasht, Iran

[b]Department of Engineering Science, Faculty of Technology and Engineering East of Guilan, University of Guilan, Rudsar, Iran

PAPER INFO

Article history:
Received: 03/Dec/2023
Revised: 22/Mar/2024
Accepted: 30/Jun/2024

Keywords:
ZnO-gC_3N_4 nanocomposite,
Photocatalyst,
Methylene blue,
Photocatalytic degradation.

ABSTRACT

In this research, zinc oxide nanoparticles were synthesized by the chemical precipitation method, and graphite carbon nitride was synthesized by the thermal decomposition method. Nanocomposites of zinc oxide co-doped with g-C_3N_4 were prepared using the Ultrasonic method. The samples were characterized by X-ray diffraction (XRD), field emission scanning electron microscope (FESEM), Fourier transform infrared spectroscopy (FT-IR), and diffuse reflectance spectroscopy (DRS). The XRD results revealed that zinc oxide and graphite carbon nitride have a hexagonal wurtzite structure and a hexagonal structure, respectively. It was found that the particle size of the ZnO/g-C_3N_4 nanocomposite was less than 100 nm. The effect of operational parameters such as concentration of doping elements, photocatalyst dosage, pH, initial concentration of Methylene Blue, effect of oxidants, and irradiation time on the extent of degradation was investigated. The photocatalytic activity of the undoped ZnO, g-C_3N_4, and ZnO/g-C_3N_4 nanocomposite photocatalysts were evaluated by the photocatalytic degradation of methylene blue in an aqueous solution. The results show that the photocatalytic activity of the ZnO/g-C_3N_4 photocatalyst is much higher than that of undoped ZnO. The cooperation of the g-C_3N_4 leads to the narrowing of the band gap and greatly improves the photocatalytic activity. The ZnO/g-C_3N_4 photocatalyst 15 mol% shows the best photoactivity and photodecomposition efficiencies were improved by 95% under Visible irradiation approximately compared with the pure ZnO sample.

DOI: https://doi.org/10.22075/chem.2024.32402.2229

[*] **.Corresponding author:** Associate Professor of Inorganic Chemistry, *E-mail address: Fallah.m@guilan.ac.ir*

How to cite this article: Tondkar Mobaraki, M., Zavvar Mousavi, H., Fallah Moafi, H., & Moghadam, M. (2024), Synthesis of Zinc Oxide-based nanocomposites for photocatalytic removal of contaminant. *Applied Chemistry Today*, **19(73)**, 73-90. (in Persian)

1. Introduction

In recent decades, the growing problem of organic water pollution has become a major cause for concern. Sources of pollution include industrial wastewater, agricultural chemicals, domestic wastewater, and marine oil spills [1]. The presence of organic dyes in aquatic environments can have harmful effects on aquatic life, which can in turn impact human health [2]. In response, semiconductor-based photocatalysis has emerged as a potential treatment method, attracting global attention due to its unique cleaning processes [3]. Photocatalysis is an advanced oxidation process (AOP) that offers several advantages for water and air purification, making it an efficient technique [4]. Metal oxide semiconductor photocatalysts, such as ZnO, have proven to be highly effective for decontaminating both air and water through heterogeneous photocatalytic oxidation. This technique is a powerful tool for removing pollutants and impurities and has been widely adopted in various industries and applications [5]. Out of the different types of nanosized metal oxides, ZnO shows great promise as a semiconductor material. This is because it has excellent environmental stability, high absorption of UV light, and is relatively inexpensive compared to other binary nanosized metal oxides [6]. Zinc oxide (ZnO) is a popular photocatalyst for the removal of pollutants in water or air, thanks to its chemical stability, non-toxicity, and high photocatalytic activity, despite having a large band gap (3.37 eV). However, ZnO's photocatalytic efficiency has often been limited by the fast recombination of photogenerated electron-hole pairs and its restricted photoresponding range. To overcome these limitations, several strategies have been proposed, including structural design, noble metal loading, ion doping, and semiconductor coupling, to extend the light absorption range or suppress the electron-hole recombination of ZnO [7,8]. Carbonaceous materials, such as activated carbon, carbon nanotubes, and graphene, are of great interest due to their unique pore structure, electronic properties, adsorptive capacity, and acidity [9]. Graphitic C_3N_4 (g-C_3N_4) has attracted significant attention among the vast majority of semiconductor photocatalysts due to its excellent light harvesting, high mechanical strength, and high thermal and photochemical stability, as well as its non-toxic properties [10–13]. Graphene-based materials have been extensively developed for the removal of water pollutants using technologies such as adsorption and photocatalytic degradation [14].

Methylene blue is a commonly used dye in various industries, including textiles, paper, rubber, plastics, leather, cosmetics, pharmaceuticals, and food [15]. However, effluents discharged from these industries often contain residues of dyes, and even extremely low concentrations can be highly visible. Discharging colored wastewater without proper treatment can lead to a range of problems, including an increase in chemical oxygen demand (COD) in the water body and an increase in toxicity [16–18]. Methylene Blue (MB) is widely used for studying photodegradation due to its beneficial characteristics. It exhibits high sensitivity to light, particularly in the visible range, making it suitable for evaluating photocatalytic processes. MB is chemically stable, allowing precise measurement of degradation rates and ensuring that observed changes result from photocatalysis rather than spontaneous decomposition [19–21]. Its strong absorption in the visible spectrum, particularly around 665 nm, enables convenient monitoring of concentration changes using techniques like UV-Vis spectroscopy [22]. MB serves as a representative model compound, sharing similarities in structure and reactivity with organic pollutants found in wastewater and environmental contaminants. The study of MB degradation provides valuable insights

into the effectiveness and applicability of photocatalysts for treating other organic pollutants [23].

This study reports the synthesis of a ZnO/g-C_3N_4 nanocomposite and its application in the photocatalytic removal of MB from wastewater under visible light. The effects of various operating parameters, including photocatalyst dosage, pH, reusability, initial MB concentration, oxidant concentration, and irradiation time, were investigated to determine their impact on MB removal efficiency. These findings offer valuable insights for the optimization of photocatalytic processes and the development of more efficient wastewater treatment technologies.

2. Experimental

2.1. Materials

All reagents used in this study were purchased from Merck (Germany) and were used without further purification. These reagents include Zinc acetate dihydrate ($Zn(Ac)_2{\cdot}2H_2O$), Urea ($CO(NH_2)_2$), Sodium Hydroxide (NaOH), Hydrochloric acid (HCl), Ammonium persulfate ($(NH_4)_2S_2O_8$), Hydrogen peroxide (H_2O_2), Potassium iodate (KIO_3), Potassium bromate ($KBrO_3$), Acetone (C_3H_6O), Ethanol (C_2H_6O) and Methylene Blue.

Table 1. Materials

name	chemical formula	molecular mass (g/mol)
Zinc acetate dihydrate	$(Zn(Ac)_2{\cdot}2H_2O)$	219.49
Urea	$(CO(NH_2)_2)$	60.06
Sodium hydroxide	(NaOH)	40.00
Hydrochloric acid	(HCl)	36.46
Ammonium persulfate	$((NH_4)_2S_2O_8)$	228.18
Hydrogen peroxide	(H_2O_2)	34.01
Potassium iodate	(KIO_3)	214.00
Potassium bromate	$(KBrO_3)$	167.00
Acetone	(C_3H_6O)	58.08
Ethanol	(C_2H_6O)	46.08
Methylene blue	$(C_{16}H_{18}N_3SCl)$	319.85

2.2. Synthesis of g-C_3N_4

Urea powder (10.0 g) was heated at a rate of 3 °C/min to a temperature of 550 °C and held at that temperature for 3 hours (Fig. 1). The resulting product was obtained in powder form and consisted of g-C_3N_4 materials [24].

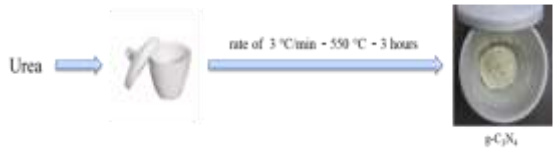

Fig. 1. Synthesis of g-C_3N_4

2.3. Synthesis of ZnO nanoparticles

The chemical precipitation method process involves the use of $Zn(CH_3COO)_2.2H_2O$ as the salt precursor and NaOH as the reducing agent to prepare Zinc Oxide nanoparticles (Fig. 2). To start, 0.01 mol of $Zn(CH_3COO)_2.2H_2O$ was dissolved in 50 mL of distilled water and stirred for 20 min. Separately, 0.02 mol of Sodium hydroxide (NaOH) solution was mixed with 50 mL of distilled water and agitated under a gentle magnetic stirrer for 20 min. The NaOH solution was then slowly added drop by drop to the $Zn(CH_3COO)_2.2H_2O$ solution until the pH reached 9-10, and the mixture was stirred continuously for 30 min, resulting in the formation of gel-like solutions. The gel-like solution was filtered (using filter paper, Buchner funnel, and vacuum pump) and washed with distilled water repeatedly until the pH reached neutral. The sample was then cured in an oven at 100°C for 2 hours and calcinated at a rate of 5 °C/min up to a temperature of 400 °C, where it was held for 3 hours [25,26].

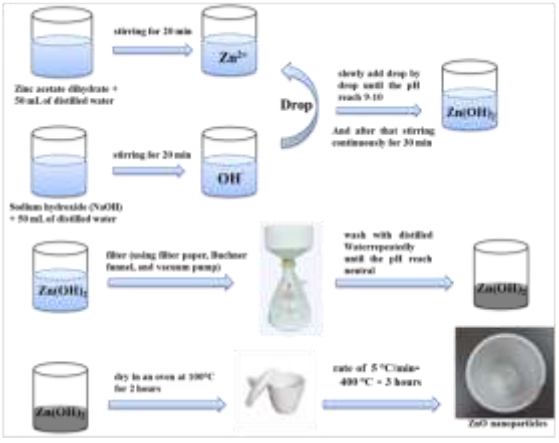

Fig. 2. Synthesis of ZnO

2.4. Preparation of ZnO/gC_3N_4 Nanocomposites

In this study, a ZnO/g-C_3N_4 nanocomposite was synthesized using an ultrasound bath (Fig. 3). Nanocomposites with varying percentages of ZnO (5, 10, 15, 20 and 25 mol%) were prepared. To synthesize the 20% mol nanocomposite, 0.4 g of ZnO nanoparticles were added to 40 mL of water and stirred for 10 minutes. The mixture was then subjected to an ultrasonic bath for 20 minutes. 0.1 g of g-C_3N_4 was slowly added to the mixture and stirred for 10 minutes. Then the mixture was again placed in the ultrasonic bath for 20 minutes. Then, the excess water in the solution was evaporated with the help of a heater and the remaining wet sediment was placed in an oven at a temperature of 100°C for 1 hour to completely dry the sediment [27].

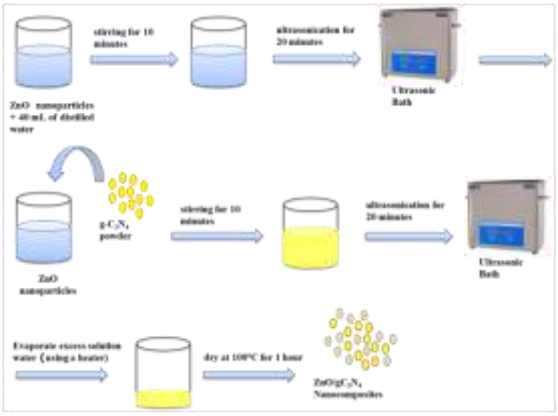

Fig. 3. Synthesis of ZnO/g-C_3N_4 nanocomposite

2.5. Photocatalytic Test Characterization Techniques

Photocatalytic activities of the synthesized ZnO/g-C_3N_4 nanocomposite were evaluated for degradation of MB under Visible irradiation (by a 392.0 W Visible lamp, SON-T 400W E E40 SL/12). The photocatalytic decomposition of MB dye was carried out in glass beakers. 20 mg of the photocatalyst was added to a 50 ml aqueous dye solution with a concentration of 10^{-5} M. During the reaction the dye solution was stirred. First, the suspension was stirred in the dark for 15 minutes to achieve adsorption equilibrium. Subsequently, the suspension was exposed to visible light at intervals of 15 minutes, and this process was continued for 1 hour. The molar amounts of MB before and after each step of irradiation were determined by measuring the absorbance at 664 nm using a spectrophotometer [28,29].

The photocatalytic decomposition was determined from the Eq. (1)

$$\text{Photocatalytic decomposition} = (C_0-C)/C_0 = (A_0-A)/A_0 \quad (1)$$

2.6. Characterization Techniques

Sample characterization was performed using various techniques such as X-ray diffraction (XRD), field emission scanning electron microscopy (FESEM), Fourier-transform infrared spectroscopy (FT-IR), and diffuse reflectance spectroscopy (DRS). To investigate the morphology and particle sizes of the ZnO and ZnO/g-C_3N_4 samples, Field Emission Scanning Electron Microscopy (FE-SEM) images were obtained. The Energy-Dispersive X-ray spectroscopy (EDS, EDXS) system was used for the compositional analysis of the doped samples. For optical properties, the UV-Visible reflectance spectra were recorded at room temperature in the reflectance mode by investigating the evolution of the absorbance.

3. Result and discussion

3.1. Characterisation of photocatalysts

3.1.1 XRD analysis

Figure 4 illustrates the powder X-ray diffraction patterns for ZnO, g-C_3N_4, and ZnO/g-C_3N_4. According to the XRD analysis results, Zinc oxide exhibits a hexagonal wurtzite crystal structure, while graphite carbon nitride has a hexagonal structure. Additionally, no impurity phases were detected in either material. In Figure 4, the diffraction peaks of pure ZnO are sharp and intense, indicating a highly crystalline sample. Conversely, in Figure 4, the diffraction peaks of g-C_3N_4 are broad and weak, suggesting a small crystal size for this sample. The XRD pattern of g-C_3N_4 exhibits two prominent

peaks at 13.24◦ and 27.66◦, corresponding to diffraction planes (100) and (002), respectively. These peaks indicate the presence of a hexagonal phase of g-C_3N_4, which was identified as JCPDS No. 01-087-1526. The weak diffraction peak at 2θ of 13.24◦ is due to repeating tri-s-triazine units arranged in a planar configuration, while the strongest diffraction peak at 2θ of 27.66◦, comparable to previously reported results, is attributed to the graphitic-like structure interlayer stacking [30,31]. The XRD pattern of ZnO nanoparticles is presented in Fig 4. The diffractions observed at 2θ values of 32.05˚, 34.70˚, 36.53˚, 47.79˚, 56.84˚, 63.08˚, 60.66˚, 68.16˚, 69.29˚, 72.75˚ and 77.17˚ correspond to the (100), (002), (101), (102), (110), (103), (200), (112), (201), (004) and (202) crystal planes, respectively. This pattern matches well with the JCDPS reference card number 080-01-0075 [32,33]. The XRD patterns of ZnO/g-C_3N_4 photocatalysts are nearly identical to that of pure ZnO, indicating that the crystal structure remains unchanged after the co-doping process with ZnO and g-C_3N_4. The XRD pattern of ZnO/g-C_3N_4 did not exhibit any detectable peaks corresponding to a separate dopant phase. This may be due to the low concentration of g-C_3N_4, which could not be distinguished as a separate phase. G-C_3N_4 may have been distributed within the lattice of ZnO, resulting in only the reflections of ZnO's hexagonal wurtzite crystal structure being observed in the XRD patterns. The doping of g-C_3N_4 was found to decrease the grain size and increase the surface area of the nanocomposite. The average grain size was calculated using Scherrer's equation, which is based on the full width at half-maximum (FWHM) of the peak of the compounds. The sizes of the ZnO and g-C_3N_4 nanoparticles, as well as the ZnO/g-C_3N_4 nanocomposite, were measured as 33.06 nm, 12.93 nm, and 28.15 nm, respectively.

$D = 0.89\lambda / \beta \cos\theta$ (2)

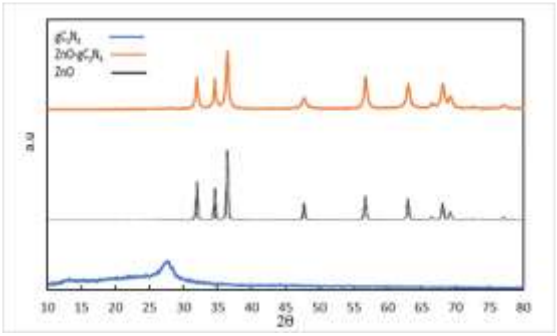

Fig. 4. XRD pattern for of ZnO, g-C_3N_4, and ZnO/g-C_3N_4 nanocomposite

3.1.2 Morphology and Compositional Analysis

The morphology and particle sizes of the ZnO and 15 mol% ZnO/g-C_3N_4 samples were analyzed using scanning electron microscopy. Figure 5 shows the scanning electron micrographs of the ZnO and ZnO/g-C_3N_4 nanocomposite. The scanning electron microscopy (SEM) images in Fig. 5(a) and Fig. 5(b) demonstrate that both ZnO nanoparticles and ZnO/g-C_3N_4 nanocomposite have an average size of less than 100 nm. The morphology of these samples is characterized by agglomerates of primary particles with an irregular shape.

An energy-dispersive X-ray (EDX) spectroscopy analysis was performed to determine the chemical composition of the synthesized ZnO/g-C_3N_4 nanocomposites. Figure 6 displays the EDX spectroscopy results for the 15 mol% ZnO/g-C_3N_4 sample, which clearly show the presence of Zn, O, C, and N elements. The spectrum reveals the existence of Zn-O-C and N, indicating that the nanocomposites are composed of Zinc and doping elements.

3.1.3 UV-Visible Diffuse Reflectance Spectra (DRS)

UV-Visible diffuse reflectance spectroscopy provides valuable insight into the interactions between photocatalyst materials and photon energies. Figure 7 illustrates the reflectance spectra of ZnO, g-C_3N_4, and a 15 mol% ZnO/g-C_3N_4 nanocomposite.

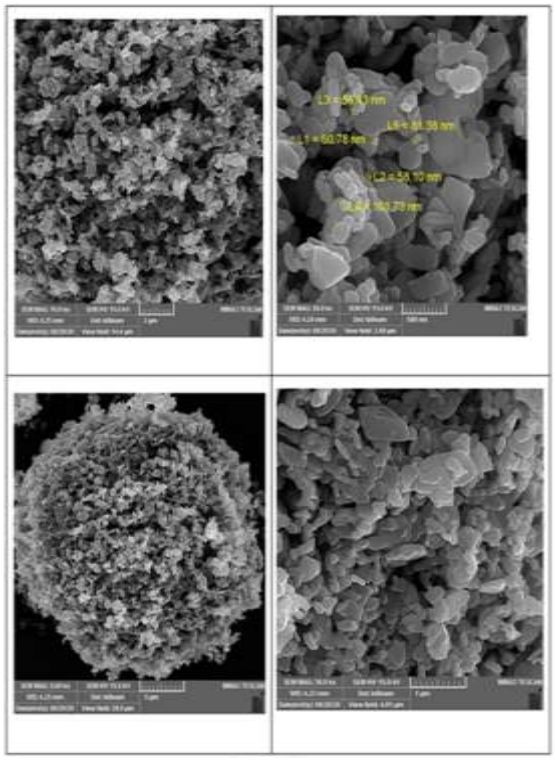

(a)

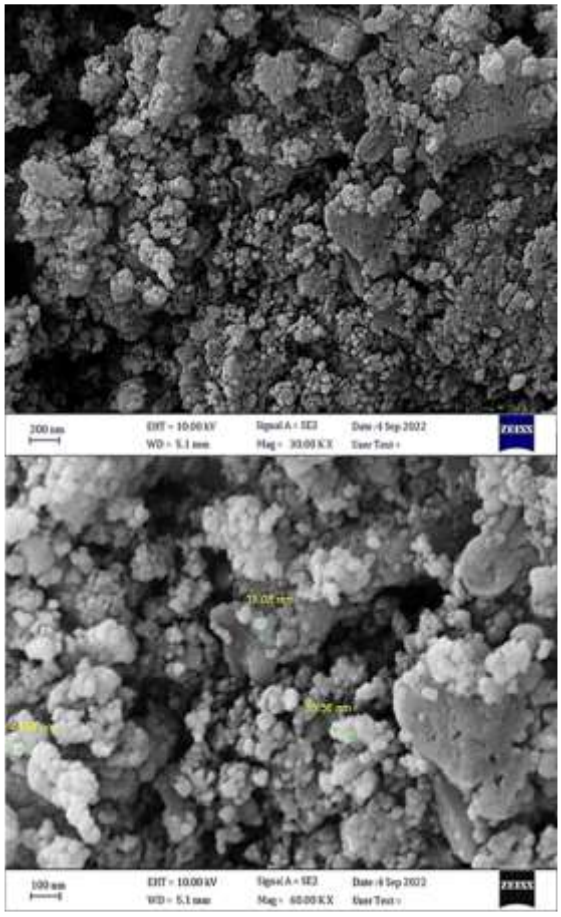

(b)

Fig. 5. Scanning electron microscopy (SEM) images of (a) ZnO nanoparticles and (b) ZnO/g-C_3N_4 nanocomposite

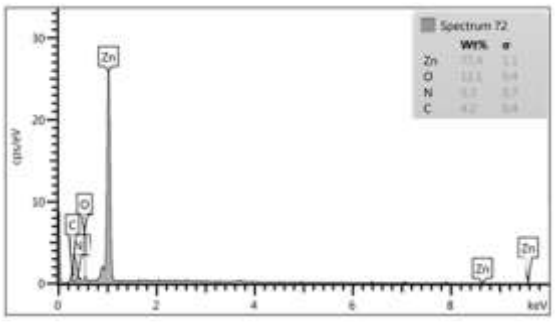

Fig. 6. Energy-dispersive X-ray (EDX) spectroscopy of the synthesized ZnO/g-C_3N_4 nanocomposites

The results show that the absorption edge of pure ZnO occurs at approximately 387.54 nm, corresponding to a band gap energy of 3.20 eV. In contrast, the absorption edge of the ZnO/g-C_3N_4 nanocomposite is shifted towards longer wavelengths, occurring at approximately 451.17 nm, which corresponds to a narrower band gap energy of 2.74 eV. Pure ZnO exhibits strong light absorption at 387.54 nm and no absorption in the visible light range. However, in the ZnO/g-C_3N_4 nanocomposite, the addition of g-C_3N_4 causes a shift in optical absorption edge towards the visible region. This shift towards longer wavelengths is attributed to the band gap narrowing of Zinc oxide due to the incorporation of g-C_3N_4. As a result, the absorption spectrum of ZnO in the nanocomposite extends from 387.54 nm to 451.17 nm, encompassing the visible region. These findings demonstrate that the addition of g-C_3N_4 significantly alters the absorption spectrum of ZnO in the nanocomposite. The band gap energy of the doped and co-doped samples can be determined by applying Eq. (3), where λ represents the wavelength (nm) of the exciting light.

$$(\alpha \cdot h\nu)^{1/\gamma} = B(h\nu - Eg) \quad (3)$$

3.1.4 Fourier-transform infrared spectroscopy (FTIR)

Figure 8 displays the FT-IR spectra of the powder samples, which were recorded in the range of 4000 to 400 cm^{-1}.

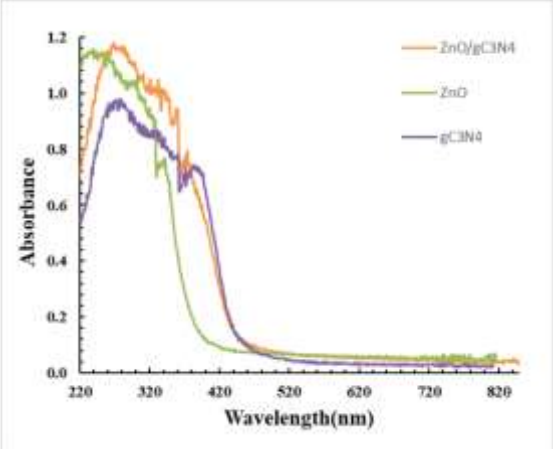

(a)

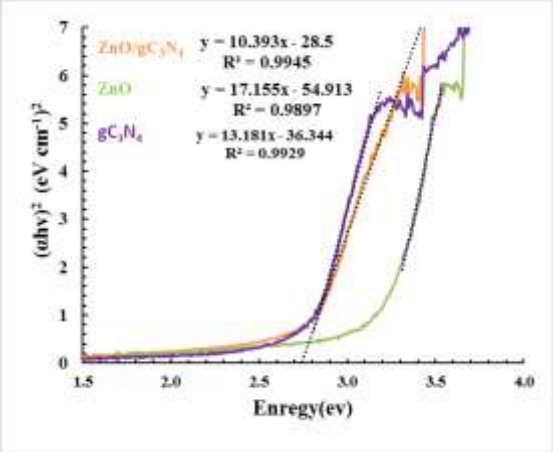

(b)

Fig. 7. (a) Diffuse reflectance spectra of ZnO, g-C_3N_4, and 15 mol% ZnO/g-C_3N_4 nanocomposite and (b) corresponding Tauc plots

The spectra exhibit a prominent absorption band at 3426 cm^{-1}, attributed to the stretching vibration of non-chemically bonded OH groups, and a band at 1632 cm^{-1}, assigned to the bending vibrations of H-O-H. Additionally, the absorption band around 1411 cm^{-1} corresponds to the bending vibration of C-H stretching. The peaks observed at 427 to 505 cm^{-1} are attributed to the Zn-O stretching vibrations.

The peaks at 1638 cm^{-1} and 1243 cm^{-1} correspond to the C=N and C–N stretching vibrations in g-C_3N_4, respectively. The sharp absorption peak centered at approximately 810 cm^{-1} is attributed to the characteristic breathing mode of tri-s-triazine cycles. In addition, the absorption band at 889 cm^{-1} can be assigned to the deformation mode of N-H in amino groups. The broadened peaks observed between 3192 cm^{-1} are related to the stretching vibrations [34,35].

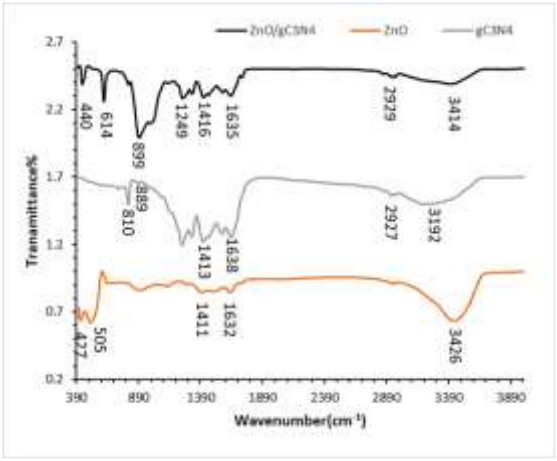

Fig. 8. FTIR spectra of ZnO, g-C_3N_4, and 15 mol% ZnO/g-C_3N_4 nanocomposite

3.2. Visible Light-Induced Photocatalytic Activity Studies

3.2.1 Photodegradability of Methylene Blue (MB)

To evaluate the photocatalytic activity of the samples, MB was selected as a model contaminant in the photocatalytic experiments. In the absence of ZnO, direct Visible irradiation did not cause any degradation of the MB concentration. However, in the presence of ZnO and the absence of Visible light, the MB concentration remained stable, and adsorption was identified as the cause of the decrease in MB concentration. To test the photolysis of a 50 ml 10^{-5} M MB aqueous solution, a pure ZnO photocatalyst was utilized. The results showed that the MB was degraded by approximately 24% in an hour upon irradiation with Visible light in the presence of ZnO, as depicted in Figure 9. These findings indicate that the photocatalytic reactions were initiated by the photocatalyst in conjunction with light irradiation, resulting in the degradation of the MB aqueous solution.

3.2.2 Effect of Concentration of Doping Elements

Figure 10 displays the results of a study on the photodecomposition of MB over ZnO/g-C_3N_4 with different concentrations of ZnO under visible irradiation.

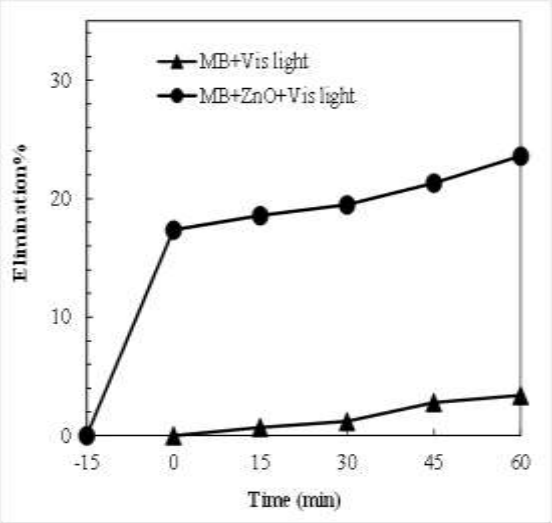

Fig. 9. The photodegradability of MB was studied in both the absence and presence of ZnO (Experimental conditions: pH = 7, catalyst weights= 60 mg, dye concentration = 1×10^{-5} M and irradiation time = 60 min)

Doping g-C_3N_4 with ZnO can alter the efficiency of the material by acting as a mediator of interfacial charge transfer or a recombination center. The efficiency of photodecomposition can be influenced by various factors such as preparation method, doping concentration, the energy level of the dopant within the ZnO lattice, and the distribution of the dopant in the particle. Therefore, the optimal concentration of dopant can vary [36,37]. In Figure 10, all the co-doped samples exhibit considerably higher photodecomposition activity compared to pure ZnO. For the co-doped ZnO/g-C_3N_4 photocatalysts, the photocatalytic activities increase with increasing concentration of doping elements. The optimal concentration of doping elements is 15 mol% for the maximum photodecomposition of MB. The ZnO dopant can function as a charge trap, slowing down the electron-hole combination rate and improving the interfacial charge transfer to degrade the MB within the appropriate concentration range of dopant (15 mol%). However, when the concentration of dopants is too high, the recombination rate will increase [36,37].

3.2.3 Effect of Solution pH

The photocatalytic degradation of MB was tested at various pH values ranging from 3 to 9. The degradation rate was observed to be highest at pH=9 (Fig. 11).

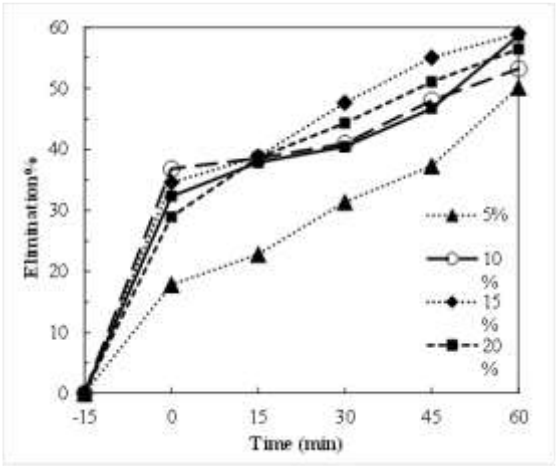

Fig. 10. The photodegradation of MB in the presence of ZnO/g-C_3N_4 was investigated under visible irradiation at varying ZnO concentrations. (Experimental conditions: pH = 7, catalyst weights= 60 mg, dye concentration = 1×10^{-5} M and irradiation time = 60 min)

The higher degradation rate at pH=9 and decreased rates at lower pH can be attributed to the Point of Zero Charge (PZC) of ZnO. The PZC of ZnO was reported as 8, which means that the ZnO surface is positively charged below pH=8, whereas it is negatively charged under alkaline conditions (pH > 8) due to adsorbed OH^- ions. The presence of a large amount of OH^- ions on the ZnO surfaces at pH=9 as well as in the reaction medium promotes the formation of $^{\bullet}OH$. It has been confirmed that $^{\bullet}OH$ are easily produced in an alkaline solution by oxidizing OH^- available on photocatalyst surfaces, thus enhancing the efficiency of the degradation process. Additionally, the electrostatic attraction between the catalyst and MB (a cationic dye) results in an increase in both adsorption and the degree of photodegradation. However, the decrease in the initial rate of degradation under acidic conditions (pH < 7) may be due to the pH being lower than the PZC. The surface of ZnO is positively charged, and MB may be repelled, resulting in a decrease in the adsorption of MB. Furthermore, the lower rate of degradation at pH=3 may be attributed to acid corrosion of ZnO [37,38].

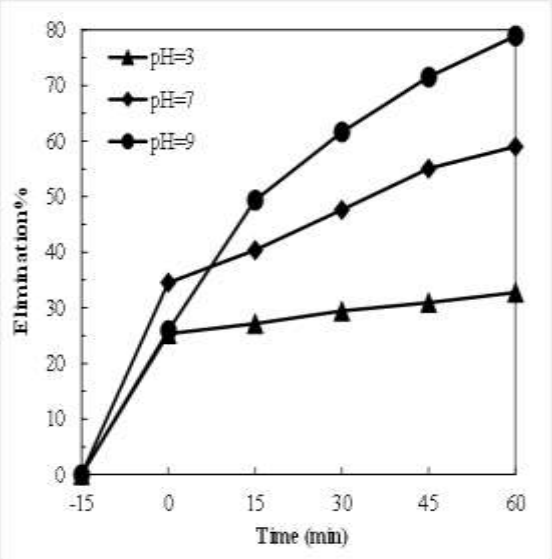

Fig. 12. Effect of pH on the photocatalytic degradation of MB in presence 15 mol% ZnO/g-C_3N_4. (Experimental conditions: catalyst weights= 60 mg, dye concentration = 1×10^{-5} M and irradiation time = 60 min)

3.2.4 Effect of Photocatalyst Dosage

This passage describes investigating the impact of the weight of ZnO/g-C_3N_4 photocatalyst on the photodegradation of the dye pollutant MB. The results (Fig. 12) indicate that while increasing the photocatalyst weight from 20 to 40 mg leads to a slight increase in the degradation rate, using 20 mg of photocatalyst is optimal due to economic and environmental concerns. However, the extent of MB degradation increases with increasing catalyst amount and reaches a maximum of 79% after 60 minutes when using 60 mg of the photocatalyst. Beyond this amount, the photoreaction rate decreases due to a decrease in visible light penetration caused by excess photocatalyst particles in the suspension and increasing opacity of the suspension. This reduces the availability of active catalytic sites for photodegradation [36,37]. Therefore, the optimal amount of the ZnO/g-C_3N_4 photocatalyst for the photodegradation of MB is 20 mg in 60 minutes. Additional experiments were conducted using this concentration of the photocatalyst.

3.2.5 Effect of Initial Concentration of Methylene Blue on the Photodegradation

This experiment focused on the photocatalytic degradation of MB at three different initial concentrations: 1×10^{-5} M, 2×10^{-5} M, and 3×10^{-5} M.

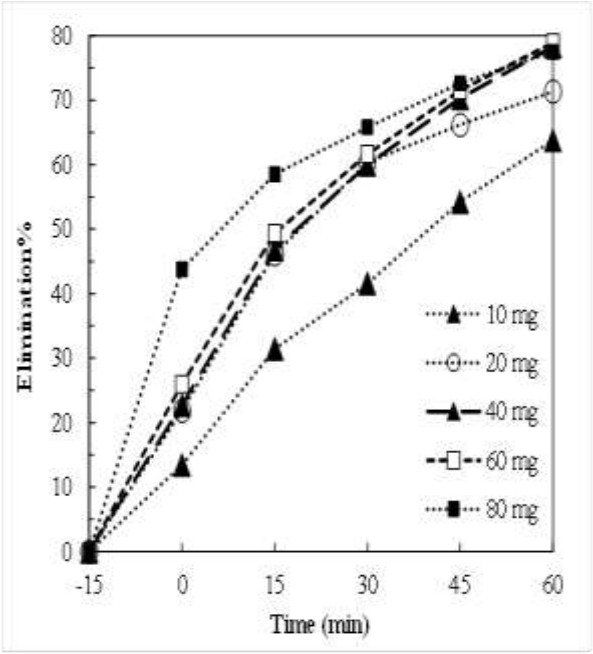

Fig. 13. Photodegradation of MB in presence different amount of 15 mol% ZnO/g-C_3N_4 under Visible irradiation. (Experimental conditions: pH = 9, dye concentration = 1×10^{-5} M and irradiation time = 60 min)

The results show that as the concentration of dye increases from 1×10^{-5} M to 3×10^{-5} M, the degradation rate decreases (Fig. 13). This behavior can be explained by the fact that as the initial concentration rises, more organic substances adsorb onto the catalytic surface, which affects the photocatalytic activity of ZnO. This, in turn, reduces the generation of hydroxyl radicals, since there are fewer active sites available for the adsorption of hydroxyl ions and the generation of hydroxyl radicals. At high dye concentrations, the active sites become covered by dye ions. Additionally, as the concentration of MB solution increases, photons get intercepted before they can reach the catalyst surface, and the path length of photons entering into the dye solution decreases. This results in a reduction in the absorption of photons by the photocatalyst and a subsequent decrease in catalytic efficiency [36–38].

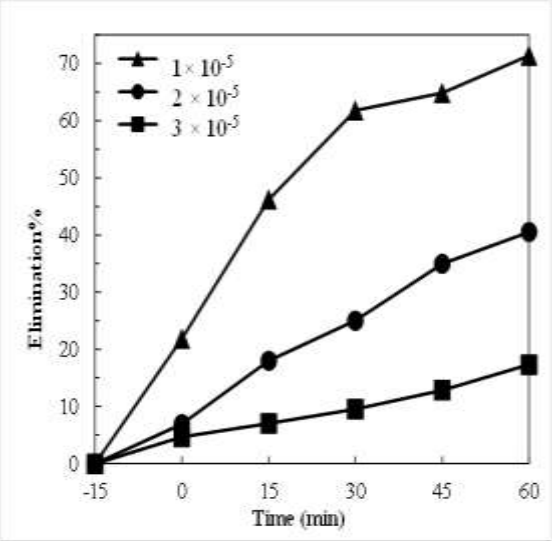

Fig. 14. The effect of initial dye concentration on the photocatalytic degradation of MB in presence of 15 mol% ZnO/g-C_3N_4 under Visible irradiation. (Experimental conditions: pH = 9, catalyst weights= 20 mg, dye concentration = 1×10^{-5} M and irradiation time = 60 min).

3.2.6 Effect of Oxidants on the Photodegradation of Methylene Blue

A study was conducted to examine the effect of different oxidants on the photocatalytic activity of ZnO/g-C_3N_4 nanocomposite. Four oxidants, namely hydrogen peroxide, ammonium persulfate, potassium iodate, and potassium bromate, were used at a concentration of 0.02 M each. The degradation rate of methylene blue dye was measured by varying the amount of oxidant added to the test medium (0.15, 0.25 and 0.4 ml). The results are presented in Figure 14. The presence of an oxidant enhanced the degradation percentage because oxidants can increase the electron-hole generation cycle and inhibit their recombination [39,40]. This results in more radicals for pollutant degradation. Among the oxidants, potassium iodate achieved the highest degradation rate of methylene blue dye at 0.25 and 0.4 ml. However, since a lower amount of oxidant is desirable, 0.25 ml of potassium iodate (0.02 M) was selected as the optimal oxidant for ZnO/g-C_3N_4 nanocomposite in the degradation of methylene blue dye.

3.2.7 Effect of irradiation time on the Photodegradation of Methylene Blue

Effect of irradiation time on the photocatalytic activity of ZnO/g-C_3N_4 nanocomposite was explored.

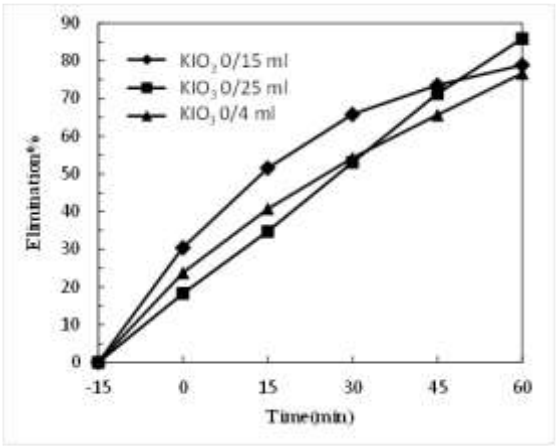

(a)

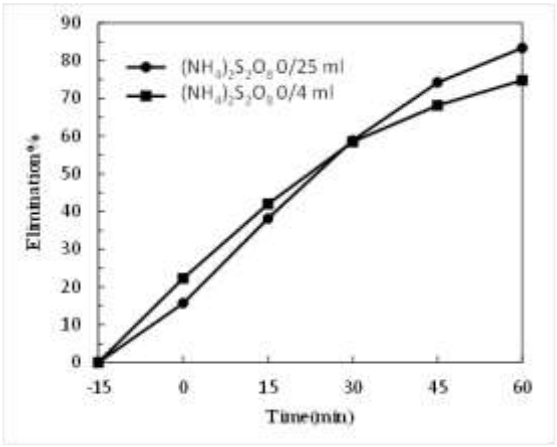

(b)

Fig. 15. The effect of initial dye concentration on the photocatalytic degradation of MB in presence of 15 mol% ZnO/g-C_3N_4 under Visible irradiation. (Experimental conditions: pH = 9, catalyst weights= 20 mg, dye concentration = 1×10^{-5} M and irradiation time = 60 min)

3.2.7 Effect of irradiation time on the Photodegradation of Methylene Blue

Effect of irradiation time on the photocatalytic activity of ZnO/g-C_3N_4 nanocomposite was explored. The photocatalyst was exposed to visible light for 60, 75, 90 and 120 minutes. The results are shown in figure 15. The data showed that the degradation of methylene blue increased with the irradiation time and the exposure of the photocatalyst to visible light. This was because more electron-holes were generated and the photocatalyst had more time to react and destroy the dye.

However, this effect reached a maximum and then increasing the time did not have a significant impact on the dye degradation. For this reason, after the degradation rate reached its maximum in 90 minutes, the increase in time had no effect and the rate of change was very slow. Based on this, 90 minutes was chosen as the optimal time.

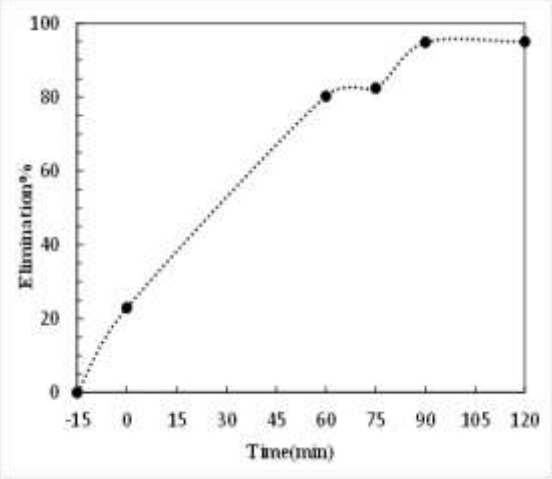

Fig. 16. Effect of irradiation time on the Photodegradation of MB in presence of 15 mol% ZnO/g-C_3N_4 under Visible irradiation. (Experimental conditions: pH = 9, catalyst weights= 20 mg, dye concentration = 1×10^{-5} M)

3.2.8 The reusability of ZnO/g-C_3N_4 nanocomposite

The reusability of the ZnO/g-C_3N_4 photocatalyst for the degradation of Methylene Blue was evaluated. A desirable feature of a photocatalyst is the ability to use it several times for dye degradation. To achieve this, the photocatalyst was separated from the test sample using a centrifuge and collected after each test. It was then washed with alcohol, acetone and water in several steps to remove the dye adsorbed on the surface of the photocatalyst. The washed photocatalyst was dried in the oven and prepared for reuse. The test conditions were kept the same in each reuse. Figure 16 shows the degradation of methylene blue by ZnO/g-C_3N_4 photocatalyst after 5 cycles. The degradation of methylene blue dye by the photocatalyst decreased from 94.78 to 88.56% in 5 consecutive uses, as shown. This decrease can be due to the blocking of some active sites of the photocatalyst that cannot be recovered [41]. However, the reduction of 6.22% in the degradation rate after 5 uses of the photocatalyst is satisfactory. The degradation efficiency still exceeds 89% after using for five cycles as illustrated in Fig. 12, which implies that the ZnO/g-C_3N_4 photocatalyst has good stability.

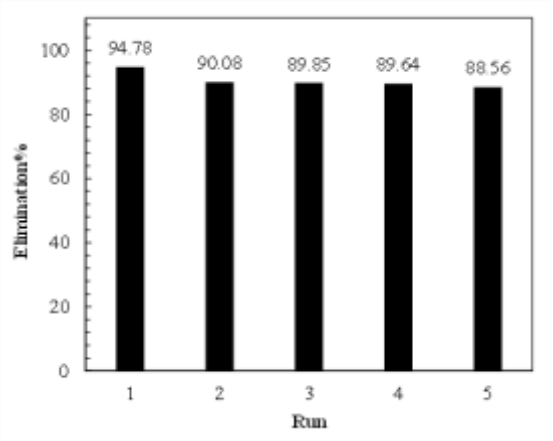

Fig. 17. The reusability of ZnO/g-C_3N_4 nanocomposite. (Experimental conditions: pH = 9, catalyst weights= 20 mg, dye concentration = 1×10^{-5} M and irradiation time = 60 min)

4. Photocatalytic mechanism

The ZnO/g-C_3N_4 nanocomposite sample resulted in enhanced adsorption and photoactivity than pure ZnO. This response could be because of two main evolutionary processes between the two variants, that is, increased surface area and smaller band gap, which support the phenomenon of synergism between adsorption and photocatalytic process (Fig. 17) [42]. The increased surface area in the case of the ZnO/g-C_3N_4 sample can provide more active sites during the photocatalytic reaction, thus producing more photogenerated electrons, and it can also lead to lower recombination of photogenerated charge carriers. The conduction band (CB) edge of ZnO (−0.5 eV) lies within the valence band (VB) (+1.4 eV) and cb (−1.3 eV) of g-C_3N_4, thus forming a temporary trapping site for photogenerated holes and electrons because of incorporated ZnO, which could trap the photo-induced electrons transferred to the CB of g-C_3N_4 from the VB under visible light irradiation. Simultaneously, holes from the VB of ZnO get injected into that g-C_3N_4 [43,44]. Thus,

$ZnO/g\text{-}C_3N_4$ could lead to improved photo-generated charge carrier separation, hence encouraging the process of interfacial electron transfer. The electron acceptors existing in the system or absorbed on the surface of ZnO, such as O_2, react with trapped electrons undergoing photoreduction to form reactive oxygen radicals $^{\bullet}O_2^-$. This is because the O_2/O_2^- redox potential lies at −0.33 eV [45]. The redox potential of $^{\bullet}OH/OH^-$ lies at +1.99, and therefore, the photogenerated holes on the $g\text{-}C_3N_4$ surface cannot react with $^{\bullet}OH^-$ or H_2O molecules to form $^{\bullet}OH$ radicals. In turn, the holes in the VB of $g\text{-}C_3N_4$ can possibly oxidize the MB dye as supported by the effect of oxidant causing hindrance to photoactivity. This improves the transfer of charge carriers, and the recombination of photo-generated e^-/ h^+ pairs is effectively delayed by ZnO doping [46]. This can be explained with equations as follows [47]:

$ZnO/g\text{-}C_3N_4 \rightarrow h\nu \rightarrow e^-/h^+$ pairs

$e^- + O^2 \rightarrow {}^{\bullet}O_2^-$

$2e^- + O_2 + 2H^+ \rightarrow H_2O_2$

$H_2O_2 + {}^{\bullet}O_2^- \rightarrow {}^{\bullet}OH + OH^- + O_2$

$h^+ + H_2O \rightarrow {}^{\bullet}OH + H^+$

$h^+ + OH^- \rightarrow {}^{\bullet}OH$

$^{\bullet}OH + h^+ + MB \rightarrow$ degradation products

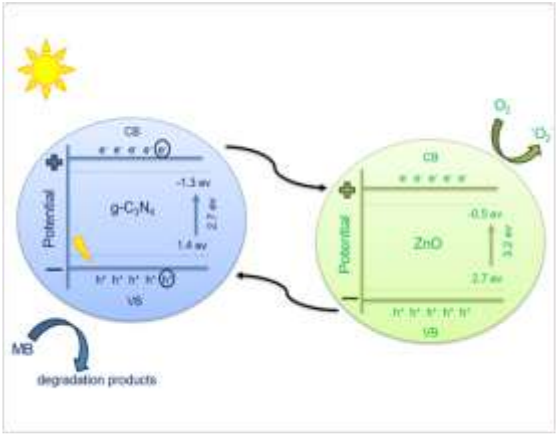

Fig. 18. Light-induced degradation of MB dye by ZnO/g-C3N4 hybrid heterojunction semiconductor photocatalyst under visible light

5. Kinetic studies of the degradation of methylene blue

In this study, the kinetics of Methylene Blue (MB) degradation using $ZnO/g\text{-}C_3N_4$ photocatalyst were investigated. Various kinetic models, including zero-order, first-order, and second-order, were examined to determine the degradation rate. Several parameters were found to influence the degradation process, such as the concentration of doping elements, photocatalyst dosage, pH, initial concentration of Methylene Blue, the effect of oxidants and irradiation time[48] .

The degradation of MB occurs in two distinct steps: the first step took place in darkness; where initial adsorption occurs; while the second step occurs in the presence of visible light. Two different approaches were taken to analyse the kinetics. In the first approach, only the data from the photocatalytic part of the experiment were considered, excluding the dark stage and absorption measurements. In the second approach, the experiment was conducted from the beginning of the dark stage until the end of the photocatalytic stage, allowing the observation of the absorption's influence on the overall change in kinetic order throughout the process (Supplementary data Table 1-5).

Based on the analysis, the photodegradation of MB was found to be best described by the pseudo-second-order model. The correlation coefficients (R^2) for the pseudo-second-order model were steadily closer to 1, indicating a better fit to experimental data which can be interpreted as larger involvement from adsorption into the overall photodegradation process.

5. Conclusions

In this study, the synthesis and characterization of Zinc oxide (ZnO) nanoparticles and graphite carbon nitride ($g\text{-}C_3N_4$) were explored for efficient photocatalytic dye degradation under visible irradiation.

1. Synthesis Methods:

- ZnO Nanoparticles: ZnO was synthesized nanoparticles using the Chemical Precipitation method. This approach allowed precise control over particle size and uniformity, critical for efficient photocatalysis.

- Graphite Carbon Nitride (g-C_3N_4): Synthesis of g-C_3N_4 involved thermal decomposition. The resulting hexagonal structure exhibited excellent stability, making it an ideal partner for ZnO in the nanocomposite.

- Co-Doped ZnO/g-C_3N_4 Nanocomposites: By combining ZnO and g-C_3N_4, nanocomposites were prepared using the Ultrasonic method. Co-doping introduced synergistic effects, enhancing photocatalytic performance.

2. Structural Analysis:

- XRD Analysis: Our X-ray diffraction (XRD) studies confirmed the hexagonal wurtzite crystal structure of ZnO. This high crystallinity ensures efficient charge transfer during photocatalysis.

- Graphite Carbon Nitride: The g-C_3N_4 material maintained a well-defined hexagonal structure, devoid of impurity phases. Its stability is crucial for sustained photocatalytic activity.

3. Morphology and Particle Sizes:

- Scanning Electron Microscopy (SEM): Detailed SEM imaging revealed that both ZnO nanoparticles and ZnO/g-C_3N_4 nanocomposites possessed an average particle size of less than 100 nm. Their irregular agglomerates contribute to unique morphological features, providing ample surface area for dye adsorption.

4. Composition:

- EDX Spectroscopy: Elemental analysis using Energy-Dispersive X-ray Spectroscopy (EDX) identified the presence of Zn, O, C, and N elements in the 15 mol% ZnO/g-C_3N_4 sample. This composition signifies successful doping of Zinc and other elements, enhancing the photocatalytic properties. The synergistic effect of co-doping contributes to efficient charge separation and utilization.

5. UV-Visible Absorption:

- Broadened Absorption Spectrum: Incorporating g-C_3N_4 into ZnO extended the absorption spectrum. The resulting nanocomposite absorbed light in the visible region (387.54 nm to 451.17 nm). This expansion allows utilization of a broader range of solar energy for photocatalysis.

The ZnO/g-C3N4 nanocomposite holds immense promise for efficient photodegradation of methylene blue (MB) under visible light. By combining the advantages of both materials—ZnO's high crystallinity and g-C3N4's stability and adsorption capacity enhanced photocatalytic performance was achieved. This finding is pivotal for environmental remediation and wastewater treatment.

Our study bridges the gap between fundamental research and practical impact, emphasizing the potential of ZnO/g-C_3N_4 as a sustainable solution. As we move forward, scalability, long-term stability, and real-world implementation should be at the forefront of further investigations. In conclusion, our research not only sheds light on the fascinating interplay of nanocomposite materials but also contributes to a cleaner and greener future. The ZnO/g-C_3N_4 nanocomposite, with its visible-light-driven photocatalytic ability, stands as a inspiration for addressing environmental challenges to explore innovative solutions that harmonize science and sustainability.

Acknowledgments

The authors would like to thank the University of Guilan for providing financial assistance for this research project.

Conflicts of Interest

The author declares that there is no conflict of interest regarding the publication of this manuscript. In addition, the authors have entirely observed the

ethical issues, including plagiarism, informed consent, misconduct, data fabrication and/or falsification, double publication and/or submission, and redundancy.

References

Springer Science & Business Media.

[1] Yu, J., Low, J., & Xiao, W. (2014). Enhanced Photocatalytic CO_2-Reduction Activity of Anatase TiO_2 by Coexposed {001} and {101} Facets. *J Am Chem Soc*, *25*(136), 8839–8842.

[2] Khataee, A.R., Karimi, A., & Darvishi, R. (2014). Europium-doped ZnO as a visible light responsive nanocatalyst: Sonochemical synthesis, characterization and response surface modeling of photocatalytic process. *Applied Catalysis A: General*, (448), 160-170.

[3] Khataee, A.R., Karimi, A., & Darvishi, R. (2014). Introduction: Titanium Dioxide (TiO_2) Nanomaterials. *American Chemical Society*, 19(114), 9281–9282.

[4] Jantawasu, P., Sreethawong, T., & Chavadej, S. (2009). Photocatalytic activity of nanocrystalline mesoporous-assembled TiO_2 photocatalyst for degradation of methyl orange monoazo dye in aqueous wastewater. *Chemical Engineering Journal*, 1(155), 223-233.

[5] Di Paola, A., García-López, E., & Marcì, G. (2012). A survey of photocatalytic materials for environmental remediation. *Journal of Hazardous Materials*, (211-212), 3-29.

[6] Zhong Shen, X., Cheng Liu, Z., & Mei Xie, S. (2009). Degradation of nitrobenzene using titania photocatalyst co-doped with nitrogen and cerium under visible light illumination. *Journal of Hazardous Materials*, 2(162), 1193-1198.

[7] Liu, Y., Hu, Y., & Zhou, M. (2012). Microwave-assisted non-aqueous route to deposit well-dispersed ZnO nanocrystals on reduced graphene oxide sheets with improved photoactivity for the decolorization of dyes under visible light. *Applied Catalysis B: Environmental*, (125), 425-431.

[8] Chen, D., Wang, D., & Ge, Q. (2015). Graphene-wrapped ZnO nanospheres as a photocatalyst for high performance photocatalysis. *Thin Solid Films*, (574), 1-9.

[9] Ahmad, M., Ahmed, E., & Hong, Z.L. (2013). A facile one-step approach to synthesizing ZnO/graphene composites for enhanced degradation of methylene blue under visible light. *Applied Surface Science*, (274), 273-281.

[10] Lv, J., Dai, K., & Zhang, J. (2015). Facile synthesis of Z-scheme graphitic-C_3N_4/Bi_2MoO_6 nanocomposite for enhanced visible photocatalytic properties. *Applied Surface Science*, (358), 377-384.

[11] Liu, J., Wang, H., & Antonietti, M. (2016). Graphitic carbon nitride “reloaded”: emerging applications beyond (photo)catalysis. *Chemical Society Reviews*, (45), 2308-2326.

[12] Dai, K., Lv, J., & Lu, L. (2016). A facile fabrication of plasmonic g-C_3N_4/Ag_2WO_4/Ag ternary heterojunction visible-light photocatalyst. *Materials Chemistry and Physics*, (177), 529-537.

[13] Huang, Q., Yu, J., & Shaowen, C. (2015). Efficient photocatalytic reduction of CO_2 by amine-functionalized g-C_3N_4. *Applied Surface Science*, (358), 350-355.

[14] Bai, S., Shen, X., & Zhong, X. (2012). One-pot solvothermal preparation of magnetic

reduced graphene oxide-ferrite hybrids for organic dye removal. *Carbon*, 6(50), 2337-2346.

[15] Han, TH., Mansoob Khan, M., & Kalathil, S. (2013). Simultaneous Enhancement of Methylene Blue Degradation and Power Generation in a Microbial Fuel Cell by Gold Nanoparticles. *Industrial & Engineering Chemistry Research*, 24(52), 8174–8181.

[16] Owamah, H., Chukwujindu, I., & Asiagwu, A. (2013). Biosorptive capacity of yam peels waste for the removal of dye from aqueous solutions. *Civil and Environmental Research*, (3), 36-47.

[17] Turhan, K., & Ozturkcan, A. (2012 Decolorization and Degradation of Reactive Dye in Aqueous Solution by Ozonation in a Semi-batch Bubble Column Reactor. *Water Air Soil Pollut*, (224), 1-13.

[18] Alkan, M., Demirbaş, O., & Çelikçapa, S. (2004). Sorption of acid red 57 from aqueous solution onto sepiolite. *Journal of Hazardous Materials*, 1(116), 135-145.

[19] Makeswari, M., & Saraswathi, P. (2020). Photo catalytic degradation of methylene blue and methyl orange from aqueous solution using solar light onto chitosan bi-metal oxide composite. *SN Applied Sciences*, (2), 336-347.

[20] Sabar, S., Abdul Aziz, H., & Yusof, N.H. (2020). Preparation of sulfonated chitosan for enhanced adsorption of methylene blue from aqueous solution. *Reactive and Functional Polymers*, 6(151), 104584.

[21] Cheng, J., Zhan, C., & Wu, J. (2020). Highly Efficient Removal of Methylene Blue Dye from an Aqueous Solution Using Cellulose Acetate Nanofibrous Membranes Modified by Polydopamine. *American Chemical Society Omega*, 10(5), 5389–5400.

[22] Mondal, S., Anda Reyes, M., & Pal, U. (2017). Plasmon induced enhanced photocatalytic activity of gold loaded hydroxyapatite nanoparticles for methylene blue degradation under visible light. *Royal Society of Chemistry Advances*, (7), 8633-8645.

[23] Khan, I., Sadiq, M., & Khan, I. (2019). One-pot solvothermal preparation of magnetic reduced graphene oxide-ferrite hybrids for organic dye removal. *Environmental Science and Pollution Research*, (26), 5140–5154.

[24] Dai, K., Lu, L., & Liang, C. (2014). Heterojunction of facet coupled g-C_3N_4/surface-fluorinated TiO_2 nanosheets for organic pollutants degradation under visible LED light irradiation. *Applied Catalysis B: Environmental*, (156–157), 331-340.

[25] Bekele, B., Degefa, A., & Tesgera, F. (2021). Green versus Chemical Precipitation Methods of Preparing Zinc Oxide Nanoparticles and Investigation of Antimicrobial Properties. *Journal of Nanomaterials*, (2021).

[26] Yang, H., Xiao, Y., & Liu, K. (2008). Chemical Precipitation Synthesis and Optical Properties of ZnO/SiO_2 Nanocomposites. *Journal of the American Ceramic Society*, 5(91), 1591-1596.

[27] Kumar, S., Baruah, A., & Tonda, S. (2014). Cost-effective and eco-friendly synthesis of novel and stable N-doped ZnO/g-C_3N_4 core–shell nanoplates with excellent visible-light responsive photocatalysis. *Nanoscale*, 9(6), 4830-4842.

[28] Asghari, A., fahimirad, B., & rajabi, M. (2017). Investigation of photo-catalytic effect of SnO_2/AC nanocomposite on photo-degradation of basic yellow 13 and rodamin b dyes. *Journal of Applied Chemistry*, 12(45), 51-58.

[29] Mahmoudi Doroh, E., Sanavi Khoshnood, R., & Sanavi Khoshnoud, D. (2023). Photocatalytic degradation of azorubine dye in aqueous solutions using Bismuth Ferrite nanopowders. *Journal of Applied Chemistry*, 18(68), 107-122.

[30] Khan, A., Tahir, M., & Bafaqeer, A. (2020). Constructing a Stable 2D Layered Ti_3C_2 MXene Cocatalyst-Assisted TiO_2/g-C_3N_4/Ti_3C_2 Heterojunction for Tailoring Photocatalytic Bireforming of Methane under Visible Light. *Energy & Fuels*, 8(34), 9810–9828.

[31] Tahir, B., Tahir, M., & Amin, N. (2017). Photo-induced CO_2 reduction by CH_4/H_2O to fuels over Cu-modified g-C_3N_4 nanorods under simulated solar energy. *Applied Surface Science*, (419), 875-885.

[32] Jurablu,, S., Farahmandjou,, M., & Firoozabadi, T. P. (2015). Sol-Gel Synthesis of Zinc Oxide (ZnO) Nanoparticles: Study of Structural and Optical Properties. *Journal of Sciences, Islamic Republic of Iran*, 3(26), 281 - 285.

[33] Poges, S., Monteleone, C., & Petroski, K. (2017). Preparation and characterization of an oxide-oxide continuous fiber reinforced ceramic matrix composite with a zinc oxide interphase. *Ceramics International*, 18(43), 17121-17127.

[34] Zhang, J., Zhang, G., & Chen, X. (2012). Co-Monomer Control of Carbon Nitride Semiconductors to Optimize Hydrogen Evolution with Visible Light. *Angewandte Chemie International Edition*, 13(51), 3183-3187.

[35] Chen, Y., Li, J., & Hong, Z. (2014). Origin of the enhanced visible-light photocatalytic activity of CNT modified g-C_3N_4 for H_2 production. *Physical Chemistry Chemical Physics*, 17(16), 8106-8113.

[36] Behnajady, M.A., Modirshahla, N., & Hamzavi, R. (2006). Kinetic study on photocatalytic degradation of C.I. Acid Yellow 23 by ZnO photocatalyst. *Journal of Hazardous Materials*, 1(133), 226-232.

[37] Sobana, N., & Swaminathan, M. (2007). The effect of operational parameters on the photocatalytic degradation of acid red 18 by ZnO. *Separation and Purification Technology*, 1(56), 101-107.

[38] Setarehshenas, N., Hosseini, S., & Esfahany, M. (2018). Photocatalytic Degradation of Basic Red 46 Azo Dye using Activated Carbon-doped ZrO_2/UV Process. *Journal of Applied Chemistry*, 13(48), 53-66.

[39] Mohammadzadeh, A., Khoshghadam-Pireyousefan, M., & Shokrianfard-Ravasjan, B. (2020). Synergetic photocatalytic effect of high purity ZnO pod shaped nanostructures with H_2O_2 on methylene blue dye degradation. *Journal of Alloys and Compounds*, (845), 156333.

[40] Rahman Setayesh, R., Nazari, P., & Askari, N. (2019). Kinetics investigation of environmental pollutants degradation using Fenton process in the presence of iron oxide nanoparticles. *Journal of Applied Chemistry*, 14(52), 183–198.

[41] Song, L., Jing, W., & Chen, J. (2019). High reusability and durability of carbon-doped TiO_2/carbon nanofibrous film as visible-light-driven photocatalyst. *Journal of Materials Science volume*, (54), 3795–3804.

[42] Wu, M., Gong, Y., & Nie, T. (2019). Template-free synthesis of nanocage-like g-C_3N_4 with high surface area and nitrogen defects for enhanced photocatalytic H_2 activity. *Journal of Materials Chemistry A*, 10(7), 5324–5332.

[43] Das, D., Banerjee, D., & Mondal, M. (2018). Nickel doped graphitic carbon nitride nanosheets and its application for dye degradation by chemical catalysis. *Materials Research Bulletin*, (101), 291-304.

[44] Tamez Uddin, M.D., Nicolas, Y., & Olivier, C. (2012). Nanostructured SnO_2–ZnO Heterojunction Photocatalysts Showing Enhanced Photocatalytic Activity for the Degradation of Organic Dyes. *Inorganic Chemistry*, 14(51), 7764–7773.

[45] Jin, R., Hu, S., & Gui, J. (2015). A Convenient Method to Prepare Novel Rare Earth Metal Ce-Doped Carbon Nitride with Enhanced Photocatalytic Activity Under Visible Light. *Bulletin of the Korean Chemical Society*, 1(36), 17-23.

[46] Tahir, H., & Saad, M. (2021). Chapter 3—Using dyes to evaluate the photocatalytic activity. In M. Ghaedi (Ed.), Interface Science and Technology (Vol. 32, pp. 125–224). Elsevier. https://doi.org/10.1016/B978-0-12-818806-4.00005-X.

[47] Jiang, F., Yan, T., & Chen, H. (2014). Ag-C_3N_4–CdS composite catalyst with high visible-light-driven catalytic activity and photostability for methylene blue degradation. *Applied Surface Science*, (295), 164-172.

[48] Jahangiri, M., tavakoly, O., & alimohammady, M. (2024). Kinetic investigation of nanophotocatalytic reaction (ZnO-Ag-Zr) in the degradation of reactive red dyes (RR198). *Journal of Applied Chemistry*, 19(70), 181-200.